Determining the 4D Dynamics of Wet Refractivity Using GPS Tomography in the Australian Region

Toby Manning, Witold Rohm, Kefei Zhang, Fabian Hurter, and Carl Wang

Abstract

The Earth's climate and weather is a highly dynamic and complex system. Monitoring and predicting meteorological conditions with a high accuracy and reliability is, therefore, a challenging task. Water vapour (WV) has a strong influence on the Earth's climate and weather due to the large energy transfers in the hydrological process. However, it remains poorly understood and inadequately measured both spatially and temporally, especially in Australia and the southern hemisphere. Four dimensional (4D) WV fields may be reconstructed using a tomographic inversion method that takes advantage of the high density of ground-based GPS Continue Operating Reference Station (CORS) networks. Recent development in GNSS tomography technique based on the dense Australian national positioning infrastructure has the potential to provide near real time 4D WV solutions at a high spatial and temporal resolution for numerical weather prediction, severe weather monitoring and precise positioning. This paper presents a preliminary study using the most advanced state CORS network—GPSnet as a test bed and introduces 4D GPS tomography in Australia and evaluates different parameters for voxel and height resolution and the influence of a priori data through simulations in a controlled field. Preliminary analyses of a real data campaign using a priori information are presented. These preliminary results conclude that the most optimal setup for GNSS tomography models in Victoria is: ~55 km horizontal resolution and 15 vertical layers with a smaller spacing in the lower troposphere and a larger spacing towards the tropopause. Further analysis will be undertaken to optimize the parameter settings for real data processing. The initial investigation into real data analysis has concluded an overall RMS error of 5.8 ppm with respect to the operational Australian Numerical Weather Prediction (NWP) model for 1 day.

Keywords

CORS • GPS • Meteorology • Tomography • Wet refractivity • WV

1 Introduction

GPS has been extensively used as a robust tool for measuring the integrated amount of WV in the atmosphere with high accuracy and under all weather conditions. It is currently regarded as one of the most important atmospheric remote sensing instruments for weather forecasting and climatology due to the rapidly increasing density of GPS CORS networks, the development of space-borne GPS technologies, and the

T. Manning (✉) • K. Zhang • C. Wang
Satellite Positioning for Atmosphere, Climate and Environment (SPACE) Research Centre, RMIT University, Melbourne, VIC 3083, Australia
e-mail: toby.manning@gmail.com

W. Rohm
Institute of Geodesy and Geoinformatics, WUELS, Wroclaw, Poland

F. Hurter
Geodesy and Geodynamics Laboratory, Institute of Geodesy and Photogrammetry, ETH Zurich, Zurich, Switzerland

C. Rizos and P. Willis (eds.), *Earth on the Edge: Science for a Sustainable Planet*, International Association of Geodesy Symposia 139, DOI 10.1007/978-3-642-37222-3_6,

continuous operability (Bevis et al. 1992; Rocken et al. 1995; Tregoning et al. 1998; Gradinarsky 2002; Bai 2005; Le Marshall et al. 2010). The capability of GPS tomography to reconstruct atmospheric wet refractivity fields has been proven in multiple studies using GNSS slant wet delays (SWDs) as the input observables (Flores et al. 2000; Nilsson 2005; Rohm and Bosy 2011; Van Baelen et al. 2011) and double difference (DD) SWDs (Nicholson et al. 2005; Troller et al. 2006; Lutz 2008; Perler et al. 2011). Current studies continue to assess the best methods to optimise the reconstruction process to ultimately attain robust algorithms with a high accuracy, reliability and near real time application.

Due to the sparse nature of ground-based atmospheric observation systems in the southern hemisphere the development of alternate methods for observing the spatial and temporal structure of the atmosphere is of high priority (Fu et al. 2009). Currently, the SPACE Research Centre at RMIT University and The Australian Bureau of Meteorology's longstanding joint collaboration has provided the research platform for the implementation of space-borne GPS meteorological information into the current NWP model (Le Marshall et al. 2010). This study aims to exploit the ground-based GPS infrastructure in Victoria and potentially other regions of Australia for the reconstruction of 4D WV distribution using GPS tomography. Detailed description of GPS signal refraction, GPS tomography principles and functional model of tomography is given in Sect. 2. The Victorian topography and atmosphere is a new area for tomographic analysis and thus a simulation study, shown in Sect. 3, is used as a first attempt to assess varying horizontal and vertical voxel resolutions and the influence of a priori data. Two synthetic horizontally homogeneous fields are used for the analysis (1) an exponentially decreasing wet refractivity field, and, (2) a spike wet refractivity field. The optimal parameters are then used for a preliminary analysis of real data, described in Sect. 4. This preliminary study is concluded in the Sect. 5, discussing implications of obtained results, presenting recommendations and showing further steps in the GPS tomography research. The outlook of this research will look at developing a robust tomographic platform providing high vertical and temporal wet refractivity data in near real time for numerical weather prediction models, severe weather prediction and precise positioning.

2 4D Modelling of Wet Refractivity with GPS Tomography

GPS satellite signals are delayed and bent due to the variations in refractive index as they propagate through different layers of the atmosphere to a ground receiver. A linear combination can effectively eliminate the ionospheric component leaving the dry and wet effects of the troposphere represented as refractivity (Rueger 2002).

$$N = 77.6890\frac{P_d}{T} + 71.295\frac{P_w}{T} + 375463\frac{P_w}{T^2} = N_{dry} + N_{wet}, \tag{1}$$

where N is the refractivity (ppm), P_d is the partial pressure of dry air (hPa), T is the atmospheric temperature (K) and P_w is the partial water vapour pressure (hPa). The first element of (1) is associated with dry refractivity N_{dry} whereas the last two with wet refractivity N_{wet}.

The GPS tomographic reconstruction process consists of retrieving the scalar field of wet refractivity values within a finite grid of volume pixels (voxels) from multiple integrated values passing through the media at different positions and orientations (Gradinarsky and Jarlemark 2004). The key aspect in GPS tomography is a linear relation between path delays which are an integrated measure of signal delay, and, refractivity N within the finite voxel model, the same relation holds. According to (1) for dry and wet refractivity, the integration of refractivity N along the propagation path delay Δ^{PD} between satellite x and receiver a can be expressed as (Troller et al. 2006):

$$\begin{aligned}\Delta^{PD}{}_a^x &= 10^{-6}\int_a^x N \cdot ds = 10^{-6}\int_a^x N_{dry} \cdot ds \\ &\quad + 10^{-6}\int_a^x N_{wet} \cdot ds = SHD + SWD,\end{aligned} \tag{2}$$

where ds is the line element along the ray path and SHD and SWD are slant dry and wet delays, respectively. Ray bending is neglected and a cut-off elevation angle of 5° is used (Bender et al. 2008).

The Bernese GPS processing software V5.0 is used to attain the Zenith Total Delays (ZTD) and the DD residuals $\Delta\Phi_{a,b}^{x,y}$ using a "shortest distance baseline" strategy and a double differencing approach (Dach et al. 2007). A DD path delay observation can be reconstructed between two satellites (x and y) and two receivers (a and b) using the ZTDs from the receivers which are mapped to the corresponding elevations of the satellites using the Niell mapping function (Niell 1996) $m\left(el_{rec}^{sat}\right)$ with the addition of DD residuals. In this study the wet refractivity is of interests, therefore the dry component is eliminated with high accuracy using additional ground meteorological observations at the GPS station using the dry Saastamoinen model (Saastamoinen 1972). The final DD SWD equation (Troller et al. 2006) reads as follows:

$$\Delta^{2,\,SWD}{}_{a,b}^{x,y} = \overline{\Delta^{2,SWD}{}_{a,b}^{x,y}} + \Delta\Phi_{a,b}^{x,y}, \tag{3}$$

where,

$$\overline{\Delta^{2,SWD^{x,y}}_{a,b}} = \left(\overline{\Delta_b^{ZWD}} \cdot m\left(el_b^x\right) - \overline{\Delta_a^{ZWD}} \cdot m\left(el_a^x\right)\right) - \left(\overline{\Delta_b^{ZWD}} \cdot m\left(el_b^y\right) - \overline{\Delta_a^{ZWD}} \cdot m\left(el_a^y\right)\right). \quad (4)$$

DD SWDs are constructed and used as the input views through the finite voxel model due to the advantage of automatically eliminating the satellite and receiver clock biases (Ware et al. 1997).

For this study, the 4D WV tomography is processed using the Atmospheric Water Vapour Tomography Software 2 (AWATOS 2) which uses a Kalman filter for the forward processing, pseudo-inverse and inter-voxel constraints (Perler 2011). Using a triliniear parameterized field the algorithm of AWATOS 2 expresses the DD SWD observations as a weighted sum of the grid nodes (Perler et al. 2011).

$$\Delta^{SWD} = 10^{-6} \sum\nolimits_i \int_{s_i}^{s_{i+1}} N_{wet,i}\, \Delta s_i \quad (5)$$

The tomography system of Eq. (5) is solved for wet refractivity using additional constraints in the form of pseudo observations, and optional a priori observations $N_{apriori}$ such as radiosonde or ground-based meteorological sensors, GPS radio occultation and radiometers. In the matrix form Eq. (5) with additional information as stated above, reads as follows (Lutz 2008):

$$\begin{pmatrix} \Delta^{2,SWD^{x,y}}_{a,b} \\ ZWD_a \\ N_{apriori,i} \\ 0_i \end{pmatrix} = H \cdot \begin{pmatrix} N_{wet\ 1} \\ N_{wet\ 2} \\ N_{wet\ 3} \\ N_{wet\ 4} \\ N_{wet\ 5} \\ N_{wet\ 6} \\ \cdots \end{pmatrix}. \quad (6)$$

Where H is the design matrix. The Kalman filter is a powerful processing procedure and is highly advantageous for estimating the evolution of dynamically changing parameters. Previous studies have also incorporated a Kalman filtering technique to efficiently utilize the slant delay observations to attain tomographic solutions (Gradinarsky and Jarlemark 2004; Nilsson 2005; Troller et al. 2006; Perler et al. 2011). Without loss of generality Kalman filter equations in epoch k, adapted to comply with notation presented before read as follows (Grewal and Weill 2002):

Predicted state vector:

$$\hat{N}_{wet\ k}\,(-) = \mathbf{F}_k \hat{N}_{wet\ k-1}(+) \quad (7)$$

Prediction covariance matrix:

$$\mathbf{P}_k\,(-) = \mathbf{F}_k \mathbf{P}_{k-1}(+)\mathbf{F}_{k-1}^T + \mathbf{Q}_{k-1} \quad (8)$$

Updated state estimate:

$$\hat{N}_{wet\ k}\,(+) = \hat{N}_{wet\ k}\,(-) + \overline{\mathbf{K}}_k \left(z_k - \mathbf{H}_k \hat{N}_{wet\ k}\,(-)\right) \quad (9)$$

Update covariance matrix:

$$\mathbf{P}_k\,(+) = \mathbf{P}_k\,(-) - \overline{\mathbf{K}}_k \mathbf{H}_k \mathbf{P}_k\,(-) \quad (10)$$

With the Kalman gain:

$$\overline{\mathbf{K}}_k = \mathbf{P}_k\,(-)\,\mathbf{H}_k^T \left(\mathbf{H}_k \mathbf{P}_k\,(-)\,\mathbf{H}_k^T + \mathbf{R}_k\right)^{-1} \quad (11)$$

Where, Q_k reflects the dynamic disturbance noise, z_k is a matrix containing all types of observations as stated in (6), P_k is the covariance matrix, F_k is the transition matrix, R_k is a measurement noise, and $\hat{N}_{\text{wet k}}\,(-/+)$ is the predicted and updated state, respectively.

Following Perler et al. (2011) the transition matrix F_k in AWATOS 2 is implemented as the identity matrix. The initial state provided from the background model is predicted with (7) and updated with (9) based on the Kalman gain matrix $\overline{\mathbf{K}}_k$ (11) in every estimation step. The procedure also applies to prediction (8) and update (10) of the covariance matrix. The initialization of the Kalman filter follows parameters set in AWATOS 2 from Perler (2011).

3 GPS Tomography Simulations

The feasibility and capability of reconstructing the physical dynamics of wet refractivity using a 4D tomographic technique above the topography of Victoria, Australia is initially tested using simulations of a synthetic tropospheric state. The simulations are then used as a preliminary evaluation for the horizontal and vertical voxel resolution, and, to assess the influence of a priori data on the solution convergence rate and solution accuracy. Future studies will focus on developing a scientific platform for near real time tomographic data in Australia. The Victorian GPS CORS network comprises approximately 105 dual-frequency geodetic grade GPS receivers in continuous operation from which 76 are used for this research. Mean inter-station distance is approximately ~55 km with a reasonably homogeneous distribution. The network is highly dense for Australian standards and has the potential to be a major resource for meteorological data especially in the absence of sufficient meteorological observation systems. The initial voxel construction was set to a standard 1° (110 km) horizontal voxel resolution. A mean GPS inter-station distance of 55 km for GPSnet was adopted as the horizontal resolution following conclusions of

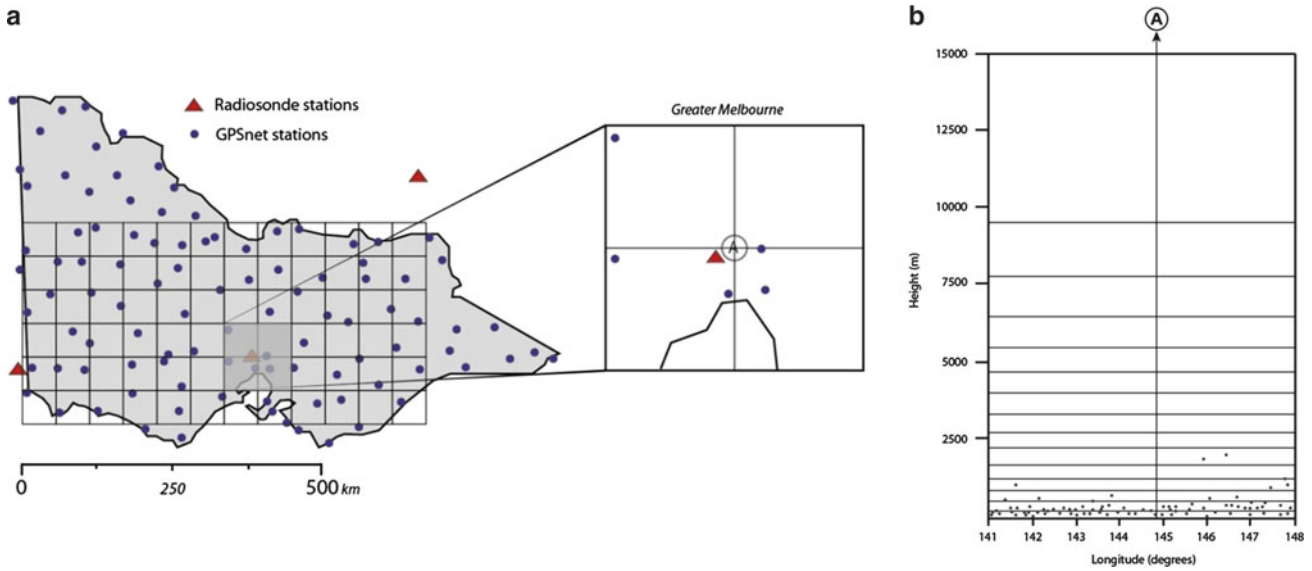

Fig. 1 3D view of the tomographic voxel model showing the first six layers (**a**). And, plan view of the GPSnet network and voxel model (**b**). Voxel corner point (A) is used for profile analysis

preconditions for GPS tomography from Bender and Raabe (2007). A final configuration of 27.5 km resolution was also tested to identify the limitations of a higher horizontal resolution, useful for analysis of severe multi cells storms, super cell storms and tropical cyclones (Ahrens and Samson 2010). Figure 1 shows the current Victorian GPSnet infrastructure and locations of sites under experiment and the base 6×12 voxel model (55 km resolution). In this analysis the voxel corner point A is used for validation purposes of the reconstructed refractivity field (Fig. 1).

3.1 Experiment Setup

Each simulation campaign is processed using real ground GPS station and satellite coordinates. Two synthetic horizontally homogeneous fields are used for the analysis (1) an exponentially decreasing wet refractivity field averaged from a radiosonde profile from 1st December 2010, and (2) a spike wet refractivity field (Perler 2011).

There is no variation in the horizontal as the main limitation in GPS tomography is the vertical resolvability (Perler 2011; Rohm and Bosy 2011). For simulations based on a synthetic exponentially decreasing wet refractivity field the following expression is used (Perler 2011):

$$N_{wet}(h) = N_{wet\,0} \exp\left(-\frac{h}{h_s}\right), \tag{12}$$

Where, $N_{wet\,0}$ is the surface wet refractivity and h_s is the scale height. To assess the impact of the vertical layer spacing on the tomographic solution two different segmentation techniques were used, namely constant and exponentially decreasing resolutions. Figure 3 presents the height distribution of GPSnet stations with respect to both layer spacing techniques.

A flat distribution of GPSnet stations is evident with only 8 stations above 500 m altitude and a maximum station height of ∼1,900 m. Large variations in receiver heights are essential for resolving the vertical structure using tomography (Bender and Raabe 2007). With the absence of optimal receiver geometry, inter-voxel constraints and additional information on the vertical profile of refractivity become increasingly more important (Gradinarsky and Jarlemark 2004). Current experiments adopt two different vertical spacing techniques—constant (Rohm and Bosy 2011) and exponential (Champollion et al. 2005; Lutz 2008; Perler 2011). This preliminary study aims to compare both methods using the same number of layers which corresponds to the same number of unknowns in (6). The exponential spacing technique distributes the stations over 7 lower layers creating a height differential which in theory will enhance the vertical resolvability compared to the constant technique which hold nearly all stations in the bottom layer.

Next step was to assess the influence of additional point observations $N_{apriori}$ on the tomographic solution. Two methods are tested (1) the $N_{apriori}$ represents simulated data for a network of synoptic weather stations, and, (2) the $N_{apriori}$ represents a simulated profile located in the centre of the model. Both methods derive observations from simulated wet refractivity field (12) and are input into the observation matrix equation set (6) as a known value with a variance of 1 ppm^2 at point $(p_{\phi,\lambda,h})$.

The evolution of the simulated tomographic reconstruction process uses a forward and backward modelling strategy. Firstly, an initial synthetic refractivity field (original field) is defined. In the forward model process, ray tracing

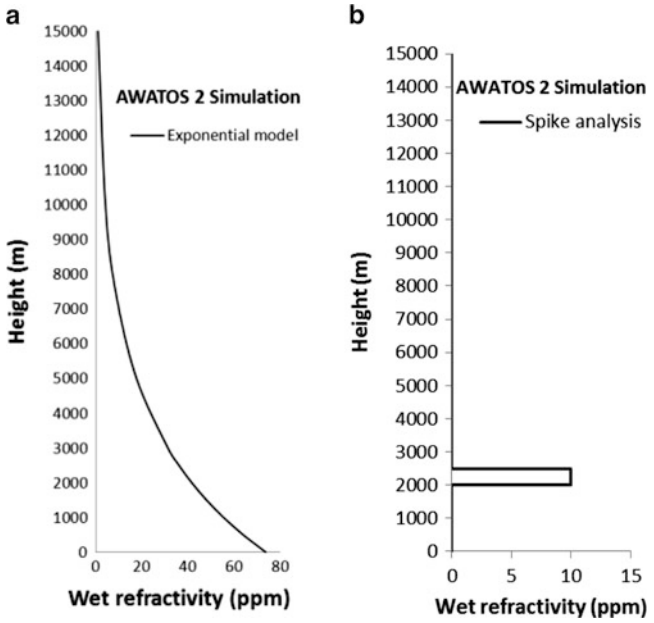

Fig. 2 Exponentially decreasing refractivity field (**a**), spike refractivity field (**b**)

Table 1 Table presenting the optimal configuration and the experiment variations

Voxel resolution	Base configuration	Experiment variations
Horizontal	6 latitude × 12 longitude	3 × 6, 6 × 12, 12 × 24
Vertical	15 levels	15
Vertical layer spacing	Exponential function	Constant, exponential function

Table 2 Observation model parameters

Observation model parameters	Value
GPS observations	Double difference slant wet delays
Number of GPS stations	74 (∼105 *in GPSnet*)
Inter-station distance (km)	∼55
GPS sampling interval size (s)	30
Tomography step size (s)	30
Additional observations	None
Observation covariance matrix	Full covariance model

implemented in the AWATOS2 software (Perler et al. 2011) is used to simulate integral *SWD* (2) and point observations through the synthetic atmosphere (12), as shown in Fig. 2. At this stage measurement noise is added to the simulation process using a Gaussian distribution error of 5 mm in the zenith direction. This accuracy measurement is extracted from final results of a validation study comparing ZPD estimates of three GPSnet receivers to three Victorian radiosonde sites over a 2 month period (December 2010–January 2011) and complies with the value used in (Perler 2011). Afterward, observations including satellite and receiver coordinates are used to reconstruct DD SWD observations table 2. The simulated observation data is then used to reconstruct the refractivity field using the Kalman filter (7–11)—this is the backward model process. Finally, the estimated field $\hat{N}_{wet}$ is compared to the simulated atmosphere N_{wet}. The step size of the backward model (9) and observation sampling size are both set to 30 s. The data evaluation process uses a profile comparison at voxel corners (A), since our focus lies on resolving the vertical structure. The root mean square (RMS) error of the difference between simulated N_{wet} profile at (A) and estimated wet refractivity profile at (A) is used to assess the accuracy of the profile solution. Additionally, the solution convergence rate and processing time are also taken into account.

3.2 Results and Discussion

Horizontal Resolution

The high horizontal voxel resolution is an imperative parameter for optimizing the depiction of highly dynamic hydrological hazards (Lutz 2008). The horizontal distribution of wet refractivity is highly variable in space and time especially during the life cycle of severe weather. The development of an optimal configuration for detecting the dynamic changes in wet refractivity in Australia is a goal for future research with potential applications in nowcasting, severe weather and precise positioning. This preliminary study compares the tomographic solution accuracy of three horizontal voxel resolutions (Table 1) using the exponentially decreasing wet refractivity state 2(a). The objective is to identify which horizontal voxel spacing is optimal for reconstructing the 4D structure of wet refractivity based on solution convergence rate, RMS error analysis and total processing time. A 3×6 configuration (110 km resolution) was used in an initial tomographic simulation. The second simulation followed Bender and Raabe (2007) where the mean GPS inter-station distance of ∼55 km was adopted (6×12). The final 27.5 km resolution was constructed as double the second resolution (12×24) to assess a higher resolution, advantageous for severe weather monitoring (Ahrens and Samson 2010). For all three horizontal resolutions vertical layer spacing is kept fixed to the exponential model (Fig. 3a). Figure 4 presents the RMS error for each configuration over the first hour. The 55 km solution converges below 1 ppm within 13 min and has a final RMS error of 0.49 ppm after 24 h. The 110 and 27.5 km solutions take 45 and 40 min respectively to converge below an RMS error of 1 ppm and conclude a final RMS error of 0.20 and 0.78 ppm respectively. The total processing time for this 24 h campaign using 27.5, 55 and 110 km, solutions were 10 h, 24 h and 5 weeks respectively.

Based on these initial results the 55 km horizontal resolution was concluded to be optimal as the convergence rate was faster than the 27.5 and 110 km solutions by more than

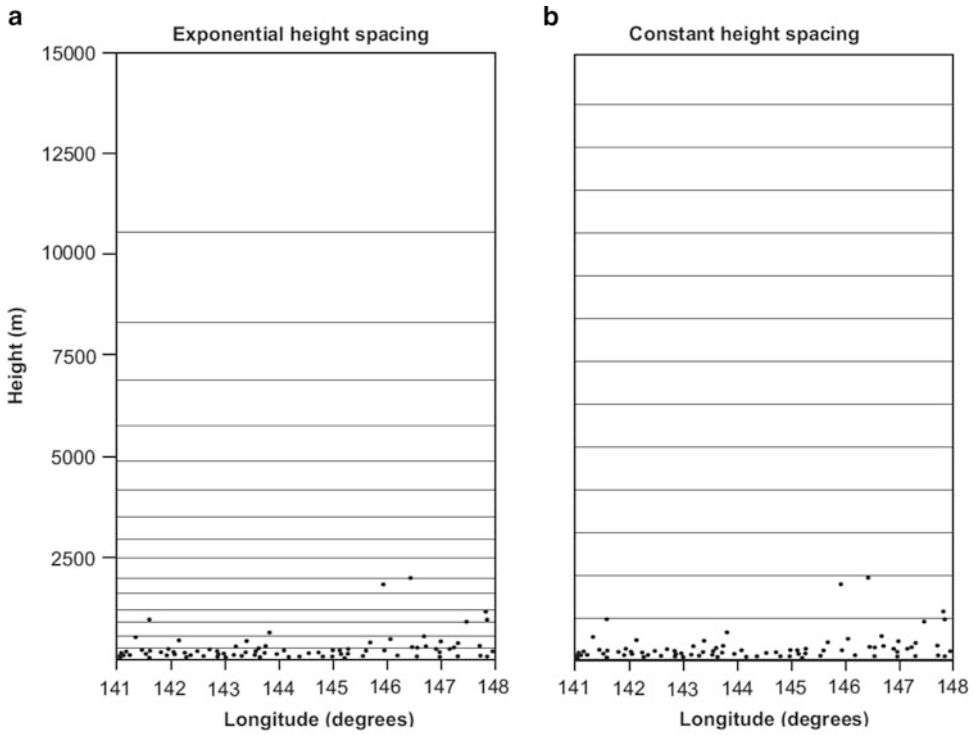

Fig. 3 Height distribution of GPSnet stations represented in of (**a**) exponential height spacing function, and of (**b**) constant height spacing

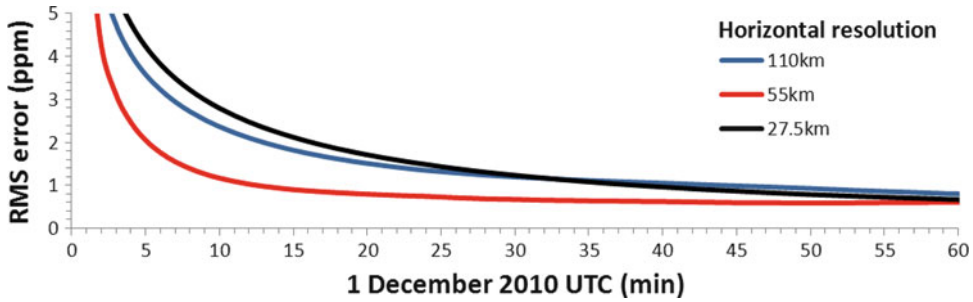

Fig. 4 Comparison of the RMS error of tomography solutions for 27.5, 55 and 110 km horizontal resolutions presenting the first 60 min of processing

a factor of 3. The processing time of the 55 and 110 km solutions were both equal to, or, less than the total campaign time which is sufficient for the scope of near real time solutions. The 27.5 km resolution was disregarded due to the processing time taking 35 times longer than the 55 km solution and the slow convergence as seen in Fig. 4.

Vertical Resolution

Up to 50 % of water vapour is located in the boundary layer. It is therefore, imperative to model the dynamic and vertical structure of water vapour below ∼2 km with high resolution. This paper presents results from a simulation study on the vertical resolution, testing the feasibility of reconstructing a sharp vertical wet refractivity spike within a defined vertical layer (Perler 2011; Rohm and Bosy 2011). This analysis uses a constant wet refractivity field of 0 ppm and implements a wet refractivity spike layer of 10 ppm from 2,000 to 2,500 m altitude situated ∼100 m beyond the altitude of the highest ground station. It compares two layer spacing techniques: constant and exponential spacing (Fig. 3). A total of 15 layers are used for each voxel spacing technique providing 1 km vertical grid spacing with the constant method and high to low vertical resolution with increasing altitude for the exponential method. DD SWD observations are simulated through the spike refractivity field (Fig. 2b).

Figure 5a presents the profile comparison between constant and exponential spacing after 20 min of processing. Both configurations produce a similar RMS of 2 ppm after 20 min, however it can clearly be seen that the exponential method has a much higher vertical resolution in the lower troposphere (< 5 km altitude) in contrast to the constant method and much less in the upper troposphere (up to 15 km). In this respect the exponential technique is advantageous as it provides high resolution at low altitudes where the density of water vapour is high and lower resolution in the upper layers where there is exponentially less. This conclusion is consistent with Lutz (2008) and Perler (2011). Figure 5b presents the convergence of the solution over time with the

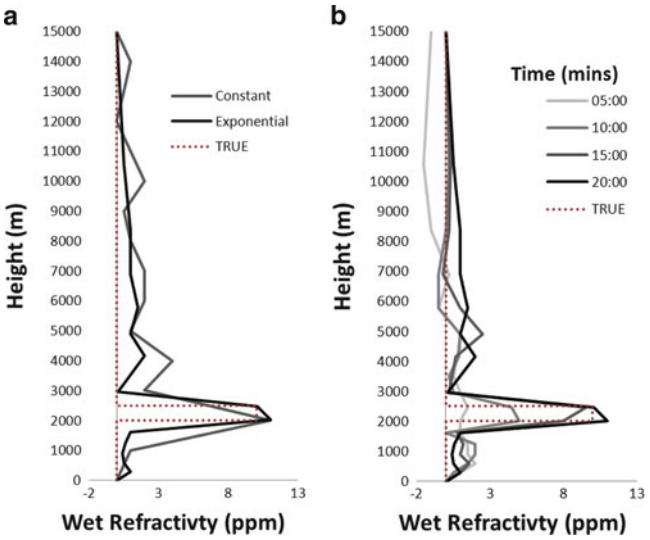

Fig. 5 Spike layer profile comparison between constant and exponential vertical spacing configurations (**a**), and time evolution of spike layer analysis using exponential vertical spacing configuration (**b**)

spike being accurately resolved after 20 min of processing using a time step and data interval size of 30 s. The optimum number of layers are yet to be determined, currently 15 layers in exponential scheme is set to comply with 1 km vertical resolution from constant method.

Additional Point Observations

Using evidence presented in this section the 55 km grid model and exponential layer function are used as the optimal grid structure. Two types of additional data are processed and compared using identical forward and backward simulation processing parameters. The first simulates the use of synoptic weather station networks within Victoria. The second simulates the inclusion of profile observations such as radiosonde and GPS radio occultation (Hajj et al. 2002). For both methods point meteorological data ($N_{apriori}$) are simulated for each station or profile point ($p_{\phi,\lambda,h}$) using (12) with a variance of 1 ppm^2 and included into the observation matrix in (6). The objective of this simulation is to identify the magnitude of influence additional data has on the solution with respect to convergence time and final RMS error accuracy. The data sampling rate for the synoptic and profile data was set to 15 min and 12 h respectively, to simulate Australian standards.

The synoptic solution converged to an accuracy of less than 1 ppm within 4 min with a final RMS error of 0.22 ppm, whereas, the profile solution converged to an accuracy of less than 1 ppm within 3 min with a final RMS error of 0.1 ppm. Compared to the solution without additional data the convergence rate for the synoptic and profile solution are faster by a factor of 3 and 4 respectively.

In addition, further developments are proposed to include both synoptic and profile data from instruments such as radiosonde and GPS radio occultation for real data campaigns. These will have significant influence on the vertical resolvability and the tomographic solution's ability to track sharp temporal changes in highly dynamic wet refractivity fields especially during the lifecycle of severe weather.

4 Preliminary Real Data Experiment

This preliminary real data experiment is conducted for 24 h on the 1st December 2010 under unstable conditions of severe weather. Hail, heavy rain and thunderstorms were all reported throughout Victoria during the 24 h campaign. GPS data from the Victorian GPS network (Fig. 2) was processed using the Bernese GPS processing software V5.0 (Dach et al. 2007) using a shortest distance baseline strategy and a double difference approach. The estimated hourly Zenith Path Delay (ZPD), the DD residuals, interpolated meteorological data from Numerical Weather Prediction model ACCESS-R (Le Marshall et al. 2010) and satellite and receiver coordinates are used to reconstruct the DD SWD (3) observations which are the primary input for the tomography inversion during each update step (7–11). Furthermore, an exponentially decreasing wet refractivity field (12) is used as the initial state. A 55 km voxel model is used with a 15 increasingly larger height layers. This preliminary study restricts the experiment to 1 day with update solutions every 5 min.

Each 6 hourly NWP analysis profile is compared to the tomographic solution with a final RMS error of 5.8 ppm. Figure 6 shows the evolution of the tomographic profile (A) up to 7,500 m throughout the 24 h with the indication of sharp temporal changes detected. The profile on the right (Fig. 6) presents the average profile for the 24 h and the standard deviation of wet refractivity at different heights. It can be seen that the largest amount of variation occurs below 3,000 m which provides the emphasis for higher resolution in lower layers. Continuing research will focus on the accurate implementation of additional a priori information from modern atmospheric sounding technologies such as GPS RO and radio sounding.

5 Conclusion and Outlook

The results presented in this paper show a new study into methods of discretizing the atmosphere in the Victorian region using a 4D GPS tomography solution processed with the AWATOS2 software package (Perler et al. 2011). The SPACE Research Centre in collaboration with the BoM are currently involved in researching sophisticated methods of

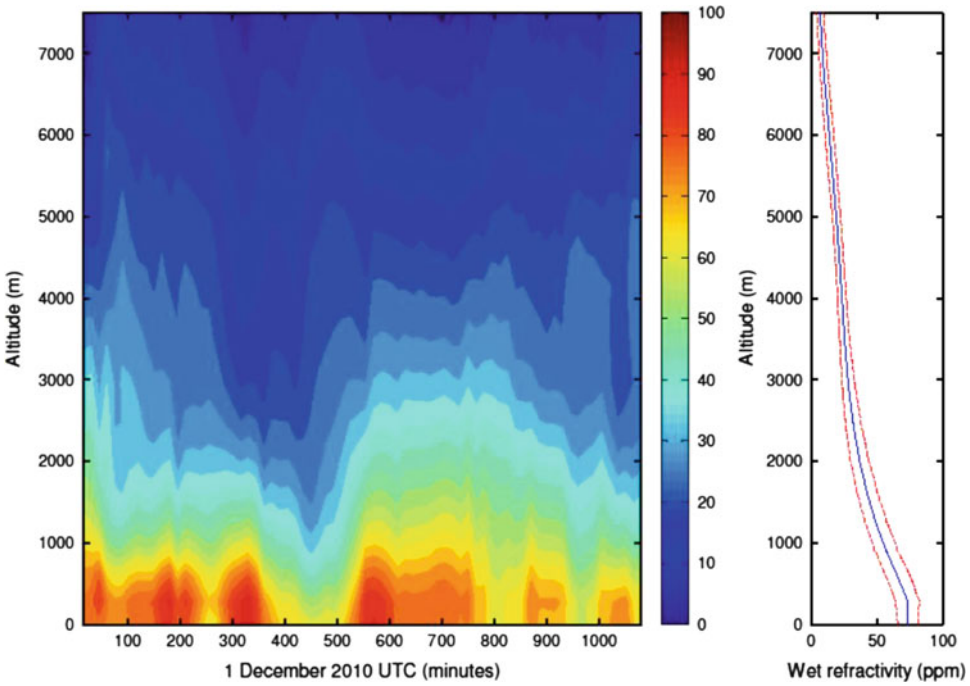

Fig. 6 Wet refractivity profile for 24 h (1st December 2010). The figure shows the temporal change of a wet refractivity profile (A) every 5 min with the profile on the right presenting the average profile and standard deviation of the daily wet refractivity at different heights

implementing space-borne GPS meteorological information into the BoM NWP model (Le Marshall et al. 2010). Ground-based GPS observations as critical Australian National Positioning Infrastructure have not yet been incorporated into the operational NWP ACCESS-R model. This preliminary study provides the platform for continuing developments in 4D GPS tomography and ultimately aims at deriving an optimized algorithm of tomography within Australia to increase the capability of NWP model forecasts, nowcasting and especially in the early detection of severe weather events. A simulation study is used to compare solution accuracies of varying horizontal and vertical voxel resolutions and the influence of a priori data. This preliminary investigation revealed an optimal voxel construction of 55 km horizontal resolution with 15 increasing height layers based on convergence rate, final RMS error and data processing time. Further simulations showed the addition of a priori information has a large influence on the vertical resolvability and convergence rate of tomographic solutions. Future simulation research will be focused on conclusive parameter optimization for the Australian region. Preliminary real data analysis assessed the time evolution of tomography solutions over 24 h with an overall RMS error of 5.8 ppm compared with Australian NWP analysis. Further real data research will aim at incorporating sophisticated a priori observation methods such as GPS RO and radiosonde into the tomography to assess the improvements in the resulting refractivity fields and the potential future capability of assimilating solutions into the Australian NWP model to analyze forecast improvements.

Acknowledgements This project is supported by the Australian Space Research Project (ASRP) and the Australian Research Council (ARC) Linkage (LP0883288) project both funded by the Australian Federal Government. We also thank the Geodesy and Geodynamics Lab, ETH Zurich, Switzerland for providing the AWATOS 2 software package, the Australian Bureau of Meteorology for providing the synoptic weather station and radiosonde data, and, the Department of Sustainability and Environment for providing the GPSnet data.

References

Ahrens D, Samson P (2010) Extreme weather and climate. Brooks/Cole Pub Co/Cengage Learning, Belmont

Bai Z (2005) Near-real-time GPS sensing of atmospheric water vapour. PhD Thesis, Queensland University of Technology

Bender M, Raabe A (2007) Preconditions to ground-based GPS water vapour tomography. Ann Geophys 25(8):1727–1734

Bender M, Dick G, Wickert J, Schmidt T, Song S, Gendt G, Ge M, Rothacher M (2008) Validation of GPS slant delays using water vapour radiometers and weather models. Meteorol Z 17(6):807–812

Bevis M, Businger S, Herring T, Rocken C, Anthes R, Ware R (1992) GPS meteorology: remote sensing of atmospheric water vapor using the global positioning system. J Geophys Res 97:15787–15801

Champollion C, Mason F, Bouin M, Walpersdorf A, Doerflinger E, Bock O, van Baelen J (2005) GPS water vapour tomography: preliminary results from the ESCOMPTE field experiment. Atmos Res 74:253–274

Dach R, Hugentobler U, Fridez P (2007) Bernese GPS software version 5.0. Astronomical Institute, University of Bern, Bern

Flores A, Ruffini G, Rius G (2000) 4-D tropospheric tomography using GPS slant wet delays. Ann Geophys 18:223–234

Fu E, Zhang K, Marion K, Xu X, Marshall J, Rea A, Weymouth G, Kuleshov Y (2009) Assessing COSMIC GPS radio occultation derived atmospheric parameters using Australian radiosonde

network data. In: The 6th international conference on mining science & technology, Procedia Earth and Planetary Science, p 1

Gradinarsky L (2002) Sensing atmospheric water vapor using radio waves. PhD Dissertation, Technical Report no. 436, Chalmers University of Technology

Gradinarsky L, Jarlemark P (2004) Ground-based GPS tomography of water vapour: Analysis of simulated and real data. J Meteorol Soc Japan 82:551–560

Grewal M, Weill L (2002) Global positioning systems, inertial navigation, and integration. Wiley-Interscience, New Jersey, pp i–xxi, 1054–1059

Le Marshall J, Xiao Y, Norman R, Zhang K, Rea A, Cucurull L, Seecamp R, Steinle P, Puri K, Le T (2010) The beneficial impact of radio occultation observations on Australian region forecasts. Aust Meteorol Oceanogr J 60:121–125

Hajj G, Kursinski E, Romans L, Bertiger W, Leroy S (2002) A technical description of atmospheric sounding by GPS occultation. J Atmos Solar-Terr Phys 64(4):451–469

Lutz S (2008) High-resolution GPS tomography in view of hydrological hazard assessment. PhD Thesis no. 17675, ETH Zurich

Niell A (1996) Global mapping functions for the atmospheric delay at radio wavelengths. J Geophys Res 101:3227–3246

Nilsson T (2005) Assessment of tomographic methods for estimation of atmospheric water vapor using ground-based GPS. PhD Thesis, Chalmers University of Technology, Göteborg

Nicholson N, Skone S, Cannon M, Lachapelle G, Luo N (2005) Regional tropospheric tomography based on real-time double difference observables. In: Proceedings of ION GNSS 2005, Long Beach, pp 269–280

Perler D, Geiger A, Hurter F (2011) 4D GPS water vapor tomography: new parameterized approaches. J Geod. doi:10.1007/s00190-011-0454-2

Perler D (2011) Water vapour tomography using global navigation satellite systems. PhD Thesis no. 20012, ETH Zurich

Rocken C, Van Hove T, Johnson J, Solheim F, Ware R, Bevis M, Chiswell S, Businger S (1995) GPS/STORM - GPS sensing of atmospheric water vapor for meteorology. J Atmos Ocean Technol 12:468–478

Rohm W, Bosy J (2011) The verification of GNSS tropospheric tomography model in a mountainous area. Adv Space Res 47:1721–1730

Rueger J (2002) Refractive index formulae for electronic distance measurement with radio and millimetre waves. School of Surveying and Spatial Information Systems, University of New South Wales, Unisurv Rep. S-68, 13 pp

Saastamoinen J (1972) Atmospheric correction for troposphere and stratosphere in radio ranging of satellites. In: Henriksen SW, Macini A, Chovitz BH (eds) The use of artificial satellites for geodesy. Geophysics monograph, vol 15. American Geophysical Union, Washington, DC, pp 247–251

Tregoning P, Boers R, O'Brien D (1998) Accuracy of absolute precipitable water vapor estimates from GPS observations. J Geophys Res 103(28):701–719

Troller M, Geiger A, Brockmann E, Kahle H (2006) Determination of the spatial and temporal variation of tropospheric water vapour using CGPS networks. Geophys J Int 167(2):509–520

Van Baelen J, Reverdy M, Tridon F, Labbouz L, Dick G, Bender M, Hagen M (2011) On the relationship between water vapour field evolution and the life cycle of precipitation systems. Q J R Meteorol Soc 137:204–223. doi:10.1002/qj.785

Ware R, Alber C, Rocken C, Solheim F (1997) Sensing integrated water vapor along GPS ray paths. Geophys Res Lett 24:417–420